Laser-induced Changes in Titanium by Femtosecond, Picosecond and Millisecond Laser Ablation

Chengjuan Yang[ab*], Yanling Tian[ab], Liangyu Cui[ab], Dawei Zhang[ab]

[a]*School of Mechanical Engineering, Tianjin University, Tianjin, 300072, China;*

[b]*Key Laboratory of Mechanism Theory and Equipment Design of Ministry of Education, Tianjin University, Tianjin 300072, China*

Chengjuan Yang*:

Postal address: School of Mechanical Engineering, Tianjin University,

92 Weijin Road, Nankai District, Tianjin, 300072, P.R.China

Telephone: (86) 18002186575, Fax: (86) 2227405561

Email: cjytju@tju.edu.cn

Yanling Tian:

Postal address: School of Mechanical Engineering, Tianjin University,

92 Weijin Road, Nankai District, Tianjin, 300072, P.R.China

Telephone: (86) 2227405561, Fax: (86) 2227405561

Email: meytian@tju.edu.cn

Liangyu Cui:

Postal address: School of Mechanical Engineering, Tianjin University,

92 Weijin Road, Nankai District, Tianjin, 300072, P.R.China

Telephone: (86) 2227405561, Fax: (86) 2227405561

Email: cuily@tju.edu.cn

Dawei Zhang:

Postal address: School of Mechanical Engineering, Tianjin University,

92 Weijin Road, Nankai District, Tianjin, 300072, P.R.China

Telephone: (86) 2287401950, Fax: (86) 2227405561

Email: medzhang@tju.edu.cn

Laser-induced Changes in Titanium by Femtosecond, Picosecond and Millisecond Laser Ablation

Abstract:

A more completed and further understanding of laser-induced material changes mechanism has a great significance to improve the controllability of laser ablation process and perfect the processing quality of final results. Therefore, comparative ablation experiments by femtosecond, picosecond and millisecond-pulsed laser were carried out on titanium in this study in order to realize the qualitative control of the laser-induced changes trend, and the quantitative control of the laser-induced changes range in titanium upon the laser irradiation with different pulse duration. Then the final surface morphology, aspect ratio, chemical composition and microstructural state of the ablated titanium were analyzed by laser scanning confocal microscopy (LSCM), X-ray photoelectron spectroscopy (XPS) and transmission electron microscopy (TEM), respectively. The dependency of the morphology, size, composition and microstructure of ablated titanium on laser pulse duration variation were emphatically discussed. It is found that, as the laser pulse duration increases from femtosecond to millisecond scale, surface morphology quality of ablated titanium gets worse, aspect ratio of microgroove decreases, proportion of titanium oxides in final ablation products becomes larger and the microstructural state of ablated titanium has a higher amorphization degree. Finally, it is deduced that the occurrence of all these experimental results can be attributed to the decreased laser intensity per pulse and enhanced heat conduction effect in titanium with the pulse duration increasing, which resulted in more serious thermal and mechanical damages in material during longer pulse duration.

Keywords: titanium; laser pulse duration variation; laser-induced change

1. Introduction

As an important metal material, titanium is a kind of metal with high specific strength, excellent corrosion resistance, good shape memory properties and biocompatibility, rare superconducting and low damping characteristics, etc *(1-4)*. Therefore, titanium becomes

Corresponding author. Email: cjytju@tju.edu.cn

a hot "star metal" and has been widely used in the fields of aerospace, defense weapons, chemical and metallurgical industries, ship manufacturing and vehicle engineering, sports fitness and rehabilitation medical devices, and some other fields. If some methods of secondary surface treatment were used, the performances of titanium can be further improved and the applicability of titanium will also be put to a new peak. There have been several methods of surface treatment to improve the surface properties of titanium, such as electroplating, electroless plating, chemical process (chemical coating), anodic oxidation process, hot dipping, vacuum plating, painting, thermal spraying, surface hardening, metallic cementation *(5, 6)*, and so on. Among these surface treatment methods, the method of laser surface treatment on titanium is gradually moving from numerous processing technologies to the fore due to its special advantages including the enhancement of the surface dependent properties (hardness, friction, fatigue, resistance to wear and corrosion), flexibility and possibility of treating small areas, leaving the others parts unaffected, and the desired firm level of adhesion bonding effect between surface layer and base material, etc *(7-9)*. All these induced positive changes in titanium aim at making material keep a lot of excellent existing features and further obtaining more expected performance. Besides the processing advantages of laser surface treatment method mentioned above, the steady developed high power lasers and their suitability introduced in production lines, laser surface treatment also encouraged the industrial application of photoelectrochemical, advanced materials, photoelectrode in dye-sensitized solar cells (DSSCs) and TiO_2 microtubes *(10-12)*.

A lot of efforts on the investigation of laser-induced changes in titanium and its alloys have been made in the past decades. Femtosecond laser treatment can produce a

richer variety of surface structures on titanium for implants and other biomedical applications than long-pulse laser treatments *(13)*. The dependences of laser-induced periodic surface structures (LIPSS) in titanium on the laser fluence and pulses number per irradiation spot have been analyzed experimentally and theoretically by femtosecond laser pulses in different environment *(14, 15)*. Those obtained experimental results were complemented by calculations based on a theoretical LIPSS model and compared to the present literature. By irradiation with ultrafast laser pulses of 130 fs duration, 800 nm wavelength in vacuum (~1mbar) or in 100 mbar He, a regular array of sharp nano-textured conical microstructures were observed on the titanium metal surface. And the reflectivity of these microstructures' surface is greatly reduced throughout the measured visible spectrum *(15)*. In addition to the study of the surface morphology, structural modification of titanium (Ti) after irradiation of femtosecond (25 fs) laser also has been explored in various pulse energies ranging. Compared with the result in dry (air) environment, surface treatment of Ti with femtosecond laser irradiation in liquid (ethanol) environment is found to allow the growth of particular surface structures in the form of grains and simultaneously induces changes in its chemical composition *(16)*. Submerging titanium target in water, A. De Bonis *(11)* observed the formation of titania nanoparticles with a certain quantity of rutile phase after a high power density configuration (2×10^{16}W/cm^2) laser ablation (Ti-sapphire, λ= 800 nm, 1 kHz, 100 fs). Upon remaining the ablated species in water, the formation of a lamellar phase could be further observed. Then a XPS analysis revealed the co-presence of Ti_2O_3, TiO_2 and TiOH, denoting the occurrence of nonstoichimetric titania phase and hence cation and oxygen vacancies *(11)*. Irradiated by a picosecond pulse laser with wavelengths of 1064 nm and 532 nm,

titanium alloy irradiated by a picosecond pulse infrared laser with a 1064 nm wavelength has better ablation surface morphology than that of the green picosecond pulse laser with a 532nm wavelength. The feature sizes are approximately linearly dependent on the laser pulse energy density at low energy density and the monotonic increase with laser pulse energy density increasing. The ablation threshold of titanium alloy irradiated by an ultra-fast pulse laser was calculated to be about 0.109 J/cm^2 *(17)*. Upon the irradiation of KrF excimer laser with wavelength 248 nm, pulse duration of 20 ns and repetition rate of 20 Hz, surface and structural properties of the laser irradiated titanium targets have been investigated under dry and wet ambient environments. The targets were exposed for various number of laser pulses ranging from 500 to 2000 in the ambient environment of air, de-ionized water and propanol at a fluence of 3.6 J/cm^2. For various number of laser pulses, the variations in the peak intensity, crystallinity and d-spacing are observed under both ambient conditions *(18)*. E. György and colleagues found that the interesting and uncommon laser-induced surface microrelief development was associated with the increase of the laser intensity effectively absorbed by the target surface as laser pulse (λ=1.064 μm, τ ≈300 ns, υ=30 kHz) number increased, where crystallization accounted for this shaped, dendritic microrelief *(19)*. In condition of ultrahigh vacuum, high purity titanium target was ablated by nanosecond pulsed Nd:YAG laser (λ=1.064 μm, τ ≈120 ns, υ=1 kHz) which induced a titanium thin film of about 250nm nominal thickness in a fcc phase deposited on a substrate with 200°C. With the increase of implanted ion fluence, structure of this titanium thin film became amorphous phase before precipitation of nanocrystalline fcc TiN phase *(20)*. While the same laser ablation process was conducted in high pressure nitrogen, the analysis result of surface layer composition of titanium

showed that the layer had a uniform surface and mainly consisted of the tetragonal δ'-TiN_x crystalline phase *(20)*. In oxygen ambient, very rapid heating-cooling process of the titanium target under energetic Nd:YAG millisecond laser pulse irradiation made the spherical nanoparticles transform from martensite into a high-pressure phase of TiO_2 with a baddeleyite-type related structure, and then into α-PbO_2-type structure *(21)*. During the situ synthesis process of TiC by laser surface treatment with pulse duration changing from 4 ms to12 ms, the dendritic morphology of composite layer changed to cellular grain structure in the conditions with the increased laser energy, low processing speed, more dissolution of carbon into liquid Ti by more heat input and positive influence of the Marangoni flow in the melted zone *(22)*. Titanium oxide nanoparticles in H_2O-distilled solvent were prepared by irradiating the titanium target with a Nd:YAG laser (second harmonic, λ=532 nm), varying the operative fluence in the range 1–8 J/cm^2 and the ablation time from 10 min to 60 min *(23)*. In the investigation on laser surface treatment of titanium alloys, a preliminary testing of the surface preparation technique using frequency tripled Nd:YAG nanosecond laser ablation (λ=355 nm) as a replacement for the chemical etch and abrasive processes has been applied to Ti-6Al-4V alloy adherends. Single lap shear testing showed that increasing laser ablation duty cycle and power not only reduced crack propagation and adhesive failure, but also increased the strength and durability *(24)*. In addition to that, using UV emitting KrCl (at 222nm, ～13 ns) and XeCl (at 308nm, ～11ns) excimer lasers, the main influences of laser beam fluence variation on Ti-6Al-4V were investigated in detail from the aspects of thermal character and surface morphology *(25)*. According to the review of previous work, a lot of efforts have been put into the research on laser-induced changes of titanium and its alloys by

laser pulses with different wavelengths, energy intensities, pulse repetition frequencies, gas atmospheres and so on *(26-28)*. However, very little attention has been paid to reveal the influence of laser pulse duration variation on the laser-induced changes in titanium.

In order to further explore the essential mechanism of laser-induced changes in titanium, surface morphology, aspect ratio, chemical composition and microstructural state changes in titanium after femtosecond, picosecond, and millisecond-pulsed laser irradiation were systematically studied in this work. Firstly, comparative ablation experiments on thin titanium plates with 1 mm thickness irradiated by femtosecond, picosecond and millisecond laser pulses were carried out at standard atmospheric pressure in air. Then laser scanning confocal microscopy (LSCM), X-ray photoelectron spectroscopy (XPS) and transmission electron microscopy (TEM) were used to analyze the surface morphology, aspect ratio, chemical composition and microstructural state changes of ablated titanium, respectively. Finally, the influence of laser pulse duration variation on the laser-induced changes in ablated titanium was analyzed intensively from the aspects of morphology, size, composition and microstructure, also the internal mechanism was discussed.

2. Experimental

Titanium plates with 1 mm thickness were selected to be the sample material in this study. All of the femtosecond, picosecond and millisecond-pulsed laser processing systems are mainly made up of optical system for generating laser pulses and motion control system for moving sample material. In optical systems, a commercially available femtosecond laser (Nd: YLF femtosecond laser system, Coherent Ltd., Libra-USP-HE), a picosecond laser (Nd: VAN HR picosecond laser system, High Q laser, picoREGENTM

SC-1064-2000 IN00060), and the JK300D millisecond-pulsed Nd:YAG laser by GSI Group were respectively used to ablate parallel microgrooves on the surface of titanium plates. Those ablated microgrooves overlapped each other to form a larger ablated region for ease of the subsequent test and analysis. All the ablation experiments were performed at standard atmospheric pressure in air. Table 1 has given the important experimental parameters in detail. It can be seen that the average laser intensities and focal spot overlapping ratios in femtosecond, picosecond, and millisecond laser ablation experiments are in the same order of magnitude. Also the wavelengths of these laser pulses are all within the range of near infrared laser wavelength. Therefore, the small differences of average laser intensities, focal spot overlapping ratios and wavelengths can be ignored in this study.

Table 1. Parameters used in laser ablation experiments

Laser type	Femtosecond laser	Picosecond laser	Millisecond laser
Wavelength (λ)	800 nm	1064 nm	1064 nm
repetition rate (f)	1000 Hz	1000 Hz	100 Hz
Pulse width	50 fs	10 ps ±1.5 ps	0.2 ms
Average power (P)	10 mW	10 mW	1 W
Scan speed (υ)	0.10 mm/s	0.10 mm/s	0.10 mm/s
Radius of the focal spot (ω)	6.24 μm	7.90 μm	100 μm
Average intensity (I_a)	8.18×10^3 W/cm^2	5.10×10^3 W/cm^2	3.1831×10^3W/cm^2
Average intensity per pulse	1.63×10^{14} W/cm^2	5.10×10^{11} W/cm^2	1.59×10^5 W/cm^2
Spot overlapping ratio (O_d)	0.9920	0.9937	0.9950

3. Results and discussion

3.1 Influence of laser pulse duration variation on the surface morphology and aspect ratio of titanium by LSCM

[Figure 1 near here]

[Figure 2 near here]

[Figure 3 near here]

LSCM (OLS4000 from Olympus) was used to observe the 2-D surface morphology and 3-D topography of the ablated region on titanium plates' surface after femtosecond, picosecond and millisecond laser ablation. From figs. 1, 2, and 3, it can be seen that surface morphology quality of the ablated titanium is overall getting worse as laser pulse duration increases. During the ultrashort pulse duration of femtosecond laser, ultrahigh laser intensity per pulse is the major reason for the good surface morphology quality of ablated microgroove. Compared with the extremely high energy input during femtosecond laser irradiation, the increase of laser pulse duration from femtosecond to picosecond and then to millisecond scale not only reduces the laser intensity per pulse of picosecond and millisecond laser, but also provides the absorbed laser energy enough time to transfer outward as heat and so the heat conduction effect in the irradiated material is significantly enhanced, which results in more serious thermal and mechanical damages including melting and solidification of irradiated material, redeposition of ablation debris, and so on. Therefore, picosecond and millisecond laser produce the microgrooves with much poorer surface morphology quality, such as worse surface smoothness, more ragged edges, and extended heat affected area (HAZ).

In addition, with the increase of laser pulse duration from femtosecond to millisecond scale, the widths and depths of microgrooves ablated by femtosecond, picosecond and millisecond-pulsed laser are 24.5μm and 10.5μm, 69.8μm and 10μm, 169μm and 18.5μm, respectively, so the corresponding aspect ratios of these microgrooves are 0.4286, 0.1433, and 0.1095, respectively. It can be found that the microgroove' aspect ratio decreases with the laser pulse duration increasing. The main reason can be attributed to the drop of laser intensity per pulse and the enhanced heat conduction effect as the laser pulse duration increases.

3.2 Influence of laser pulse duration variation on the chemical composition of titanium by XPS

[Figure 4 near here]

[Figure 5 near here]

[Figure 6 near here]

Based on the XPS analysis results shown in figs. 4, 5, and 6, femtosecond laser ablation product mainly include TiO_2, TiO_2 rutile, Ti_2O_3, TiN (loss peak), Ti, the major compositions of picosecond laser ablation product are TiO_2, TiO_2 rutile, Ti_2O_3, TiN (loss peak), Ti (C, N), $TiO_{0.73}$, and millisecond laser ablation mainly produces TiO_2 (in oxide films) and TiO_2 rutile. Replacing Ti displayed in fig. 4, the additional Ti (C, N) and $TiO_{0.73}$ appearing in fig. 5 mainly result from the relatively full reaction between air and titanium during picosecond pulse duration compared with the femtosecond laser ablation. So it can be found that, as the laser pulse duration increases from femtosecond to picosecond scale, increased pulse duration of picosecond laser induces that the type of

new generated titanium compounds becomes varied, the composition of compounds themselves gets more complex, and the content of residual elemental titanium (Ti) is gradually reduced. While for millisecond laser ablation, because of much longer pulse duration and significantly enhanced heat conduction effect, millisecond laser pulses melt the solid sample material to overheated liquid titanium, which reacts with air violently, then solidify and redeposit to produce a layer of oxide film on the material surface. This oxide film prevents air from further reacting with inside material in turn. Therefore, the oxidation reaction dominates in the interaction between millisecond laser and titanium, TiO_2 (in oxide films) and TiO_2 rutile then become the major compositions of millisecond laser ablation product.

A synthesis of above XPS results shows that the proportion of titanium oxide in final ablation product increases with the laser pulse duration increasing, which becomes a criterion to reflect the intensity of the interaction between laser and titanium, and to mirror the degree of thermal and mechanical damages in ablated titanium after laser irradiation.

3.3 Influence of laser pulse duration variation on the final microstructural states of titanium by TEM

A TEM (Philips: CM200, acceleration voltage: 2000KV) was used to analyze the microstructural state of femtosecond, picosecond and millisecond laser ablation products. Based on the principle of TEM electron diffraction pattern analysis, the TEM electron diffraction pattern of monocrystal structure is made up of many neatly arranged light spots, those of polycrystal and amorphous structures consist a series of concentric rings

with different radius and only a diffuse center light spot surrounded by one or more very diffuse diffraction rings, respectively *(25)*. TEM electron diffraction patterns of other microstructural states can be derived from above three typical patterns.

From the TEM analysis results shown in fig. 7, it can be determined that the final product of femtosecond laser and titanium ablation mainly contains the deformation structure, nanocrystalline structure, and amorphous structure. Among them, because the TEM electron diffraction pattern in fig. 7 (a) is composed of many neatly arranged light spots, the deformation structure is deduced to contain a lot of regular monocrystal structure. While for the TEM electron diffraction patterns in figs. 7 (b) and (c), the appearence of intermittent light rings indicates that the polycrystal and amorphous structures are their main structural components, in which the proportion of polycrystal structure is larger. Therefore, the final product of femtosecond laser and titanium ablation mainly consists of regular monocrystal structure, polycrystal structure and amorphous structure, and the proportion of amorphous structure is the least among these three structures.

[Figure 7 (a) near here]

[Figure 7 (b) near here]

[Figure 7 (c) near here]

Based on the TEM analysis results as shown in fig. 8, it can be confirmed that the final product of picosecond laser and titanium ablation also mainly consists of the deformation structure, nanocrystalline structure, and amorphous structure. However,

compared with the TEM results in fig. 7, the continuity of TEM diffraction rings in figs. 8 (a), (b) becomes worse and the diffusion phenomenon of TEM diffraction rings gets more obvious. Therefore, it can be deduced that those deformation structure and nanocrystalline structure in the picosecond laser ablation product are both made up of polycrystal and amorphous structures, in which the proportion of amorphous structure is higher. For the TEM electron diffraction pattern in fig. 8 (c), the occurrence of the diffuse center light spot surrounded by several very diffuse diffraction rings indicates that the amorphous structure is the major structural component of the nanocrystalline and amorphous structures. So the polycrystal structure and amorphous structure are thought to be main structural components of picosecond laser and titanium ablation product, and the proportion of amorphous structure is higher between the two structures.

[Figure 8 (a) near here]

[Figure 8 (b) near here]

[Figure 8 (c) near here]

[Figure 9 (a) near here]

[Figure 9 (b) near here]

[Figure 9 (c) near here]

[Figure 9 (d) near here]

TEM analysis results in fig. 9 display that the twin crystal, nanocrystalline structure and amorphous (particle) structure are the major final products of millisecond

laser and titanium ablation. Similar with the TEM electron diffraction pattern in fig. 7 (a), the neatly arranged light spots in fig. 9 (a) indicate that twin crystal is made up of some regular monocrystal structures. The poor continuity and diffusion phenomenon of TEM diffraction rings in fig. 9 (b) illustrate that the nanocrystalline structure is mainly composed of polycrystal and amorphous structures, in which the proportion of amorphous structure is higher. While for the TEM electron diffraction pattern in figs. 9 (c) and (d), the obvious diffuse center light spot and its surrounding diffuse diffraction rings show that the amorphous structure is the major structural component for both nanocrystalline and amorphous (particle) structures. Therefore, the regular monocrystal structure, polycrystal structure and amorphous structure are the main structural components of millisecond laser ablation product, however, the proportion of amorphous structure have the absolute predominance in content.

A comprehensive analysis on the TEM results of femtosecond, picosecond, millisecond laser and titanium ablation products reveals that polycrystal and amorphous structures are the common microstructural components of above three ablation products. Difference of the content proportion of amorphous structure in those ablation products indicates that the amorphization degree of ablated titanium intensifies as the laser pulse duration increases from femtosecond to millisecond scale, the main reason of which could be ascribed to the more and more serious thermal and mechanical damages in titanium upon the laser irradiation with longer pulse duration. Consequently, together with the proportion of titanium oxide in final ablation product, amorphization degree of ablated titanium becomes another criterion to describe the intensity of the interaction between laser and titanium, also to evaluate the degree of thermal and mechanical

damages in ablated titanium after laser irradiation.

4. Conclusions

An ultrafast melting or vaporing occurs when the sample material is heated by pulsed lasers, which rapidly results in a significant temperature gradient in the transitional region between the molten or vaporized material and its surrounding solid region. Then, an ultrafast cooling happens at the end of laser pulses irradiation. After above melting and solidification processes, sample material is endowed with some new characteristics of surface morphology, chemical composition and microstructural state. Based on the obtained analysis results by LSCM, XPS and TEM, the influence of laser pulse duration variation on the surface morphology, aspect ratio, chemical composition, and microstructural state of titanium were analyzed systematically in this study. Finally, several conclusions can be summarized as follows:

(1) With the laser pulse duration increasing from femtosecond to millisecond scale, the occurence of worsening surface morphology quality of ablated titanium and decreased aspect ratios of microgrooves can be attributed to the drop of laser intensity per pulse and the enhanced heat conduction effect which results in more serious thermal and mechanical damages in titanium.

(2) A synthetical study on the chemical composition and microstructural state of femtosecond, picoseond, millisecond laser and titanium ablation products indicates that the proportion of titanium oxide and amorphization degree of these final ablation products become the main criteria to evaluate the intensity of the interaction between laser and titanium, and also to reflect the degree of thermal and mechanical damages in

ablated material after laser irradiation. Therefore, through the investigation on oxidization and amorphization of final laser ablation products, it is possible to realize the qualitative control of laser-induced changes trend, and the quantitative control of laser-induced changes range in titanium, finally, to improve the controllability of ablation process and the quality of final processing results.

Acknowledgements, This work was supported by National Natural Science Foundations of China [Nos. 51405333, 51175372, 51275337]; Independent Innovation Fundation of Tianjin University [No. 1405]; and Open Foundation of Key Laboratory of Mechanism Theory and Equipment Design of Ministry of Education in Tianjin University.

References

(1) Oshida, Y. *Bioscience and bioengineering of titanium materials;* Elsevier: Oxford, UK, 2007.

(2) Kulka, M.; Makuch, N.; Dziarski, P.; Piasecki, A.; Miklaszewski, A. Microstructure and Properties of Laser-borided Composite Layers Formed on Commercially Pure Titanium. *Opt. Laser Technol.* **2014,** *56,* 409–424.

(3) Zhang, E.L.; Li, F.B.; Wang, H.Y.; Liu, J.; Wang, C.M.; Li, M.Q.; Yang, K. A New Antibacterial Titanium–copper Sintered Alloy: Preparation and Antibacterial Property. *Mat. Sci. Eng. C-Mater.* **2013,** *33* (7), 4280–4287.

(4) Taghavi, A.; Behfrooz, M.R. Production and Investigation About Structural Properties of Titanium Very Thin Films. *J. Appl. Sci. & Agric.* **2013,** *8* (3), 133-139.

(5) Montealegre, M.A.; Castro, G.; Rey, P.; Arias, J.L.; Vázquez, P.; González, M. Surface Treatments by Laser Technology. *Contemp. Mater.* **2010,** *I* (1), 19–30.

(6) Yun, H.G.; Bae, B.S.; Kang, M.G. A Simple and Highly Efficient Method for Surface Treatment of Ti Substrates for Use in Dye-sensitized Solar Cells. *Adv. Energy Mater.* **2011,** *1* (3), 337–342.

(7) Schuöcker, D., 1st Ed. *Handbook of the EuroLaser Academy;* Springer: Chapman & Hall, London, 1998.

(8) Steen, W.M., Watkins, K.G., 3rd Eds.; *Laser Material Processing;* Springer: New York, 2003.

(9) Tian, Y.S.; Chen, C.Z.; Li, S.T.; Huo, Q.H. Research Progress on Laser Surface

Modification of Titanium Alloys. *Appl. Surf. Sci.* **2005,** *242* (1-2), 177–184.

(10) Noh, J.H.; Park, J.H.; Han, H.S.; Lee, S.; Kim, D.H.; Jung, H.S.; Hong, K.S. *Synthesis of Hierarchically Organized Nanostructured TiO_2 by Pulsed Laser Deposition and Its Application to Dye Sensitized Solar Cells,* 2010 IEEE 3rd International Nanoelectronics Conference (INEC 2010), Hong Kong, China, Jan 3–8, 2010, 1056.

(11) Bonis De, A.; Galasso, A.; Ibris, N.; Laurita, A.; Santagata, A.; Teghil, R. Rutile Microtubes Assembly From Nanostructures Obtained by Ultra-short Laser Ablation of Titanium in Liquid. *Appl. Surf. Sci.* **2013,** *268,* 571–578.

(12) Medina-Valtierra, J.; Frausto-Reyes, C.; Ortiz-Morales, M. Phase Transformation in Semi-transparent TiO_2 Films Irradiated With CO_2 Laser. *Mater. Lett.* **2012,** *66* (1), 172–175.

(13) Vorobyev, A.Y.; Guo, C. Femtosecond Laser Structuring of Titanium Implants. *Appl. Surf. Sci.* **2007,** *253* (17), 7272–7280.

(14) Bonse, J.; Höhm, S.; Rosenfeld, A.; Krüger, J. Sub-100-nm Laser-induced Periodic Surface Structures Upon Irradiation of Titanium by Ti:sapphire Femtosecond Laser Pulses in Air, *Appl. Phys. A* **2013,** *110,* 547–551.

(15) Nayak, B.K.; Gupta, M.C.; Kolasinski, K.W. Formation of Nano-textured Conical Microstructures in Titanium Metal Surface by Femtosecond Laser Irradiation. *Appl. Phys. A- Mater.* **2008,** *90* (3), 399–402.

(16) Shazia Bashir; Shahid Rafique, M.; Chandra Sekher Nathala; Wolfgang Husinsky, Surface and Structural Modifications of Titanium Induced by Various Pulse Energies of a Femtosecond Laser in Liquid and Dry Environment, *Appl. Phys. A* **2014,** *114,* 243–251.

(17) Zheng, B.X.; Jiang, G.D.; Wang, W.J.; Wang, K.D.; Mei, X.S. Ablation Experiment and Threshold Calculation of Titanium Alloy Irradiated by Ultra-fast Pulse Laser, *AIP Adv.* **2014,** *4,* 031310.

(18) Nisar Ali; Shazia Bashir; Umm-i-Kalsoom; Mahreen Akram; Khaliq Mahmood, Effect of Dry and Wet Ambient Environment on the Pulsed Laser Ablation of Titanium, *Appl. Surf. Sci.* **2013,** *270,* 49–57.

(19) György, E.; Pérez del Pino, A.; Serra, P.; Morenza, J.L. Growth of Surface Structures

on Titanium Through Pulsed Nd:YAG Laser Irradiation in Vacuum. *Appl. Surf. Sci.* **2002,** *197-198,* 851–855.

(20) György, E.; Pérez del Pino, A.; Serra, P.; Morenza, J.L. Depth Profiling Characterisation of the Surface Layer Obtained by Pulsed Nd: YAG Laser Irradiation of Titanium in Nitrogen. *Surf. Coat. Tech.* **2003,** *173* (2-3), 265–270.

(21) Chen, S.Y.; Shen, P. Laser Ablation Condensation and Transformation of Baddeleyite-type Related TiO_2. *Jpn. J. Appl. Phys.* **2004,** *43* (4A), 1519–1524.

(22) Hamedi, M.; Torkamany, M.; Sabbaghzadeh, J. Effect of Pulsed Laser Parameters on In-situ TiC Synthesis in Laser Surface Treatment. *Opt. Laser. Eng.* **2011,** *49* (4), 557–563.

(23) Barreca, F.; Acacia, N.; Barletta, E.; Spadaro, D.; Currò, G.; Neri, F. Titanium Oxide Nanoparticles Prepared by Laser Ablation in Water. *Radiat. Eff. Defect. S.* **2010,** *165* (6-10), 573–578.

(24) Palmieri, F.L.; Watson, K.A.; Morales, G.; Thomas, W.; Robert, H.; Wohl, C.J.; Hopkins, J.W.; Connell, J.W. Laser Ablative Surface Treatment for Enhanced Bonding of Ti-6Al-4V Alloy. *ACS Appl. Mater. Inter.* **2013,** *5* (4), 1254–1261.

(25) http://www.photomachining.com/laser-micromachining-products-dpss-laser.html

(26) Milovanović, Dubravka S.; Petrović, Suzana M.; Shulepov, Mikhail A.; Tarasenko, Victor F.; Radak, Bojan B.; Miljanić, Šćepan S.; Trtica, Milan S. Titanium Alloy Surface Modification by Excimer Laser Irradiation. *Opt. Laser Technol.* **2013,** *54,* 419–427.

(27) Pérez del Pino, A.; Serra, P.; Morenza, J. Coloring of Titanium by Pulsed Laser Processing in Air. *Thin Solid Films* **2002,** *415* (1), 201–205.

(28) Krishnan, R.; Amirthapandian, S.; Mangamma, G.; Ramaseshan, R.; Dash, S.; Tyagi, A.K.; Jayaram, V.; Raj, B. Implantation Induced Hardening of Nanocrystalline Titanium Thin Films. *J. Nanosci. Nanotechno.* **2009,** *9* (9), 5461–5466.

(29) Medina-Valtierra, J.; Frausto-Reyes, C.; Ortiz-Morales, M. Phase Transformation in Semi-transparent TiO_2 Films Irradiated With CO_2 Laser. *Mater. Lett.* **2012,** *66* (1), 172–175.

Tables with captions

Table 1. Parameters used in laser ablation experiments

Laser type	Femtosecond laser	Picosecond laser	Millisecond laser
Wavelength (λ)	800 nm	1064 nm	1064 nm
repetition rate (f)	1000 Hz	1000 Hz	100 Hz
Pulse width	50 fs	10 ps ±1.5 ps	0.2 ms
Average power (P)	10 mW	10 mW	1 W
Scan speed (υ)	0.10 mm/s	0.10 mm/s	0.10 mm/s
Radius of the focal spot (ω)	6.24 μm	7.90 μm	100 μm
Average intensity (I_a)	8.18×10^3 W/cm^2	5.10×10^3 W/cm^2	3.1831×10^3W/cm^2
Average intensity per pulse	1.63×10^{14} W/cm^2	5.10×10^{11} W/cm^2	1.59×10^5 W/cm^2
Spot overlapping ratio (O_d)	0.9920	0.9937	0.9950

Figure captions

Figure 1. LSCM results of femtosecond laser ablation product

Figure 1 (a). 2-dimensional surface morphology

Figure 1 (b). 3-dimensional topography

Figure 2. LSCM results of picosesecond laser ablation product

Figure 2 (a). 2-dimensional surface morphology

Figure 2 (b). 3-dimensional topography

Figure 3. LSCM results of millisecond laser ablation product

Figure 3 (a). 2-dimensional surface morphology

Figure 3 (b). 3-dimensional topography

Figure 4. XPS result of femtosecond laser ablation product

Figure 5. XPS result of picosecond laser ablation product

Figure 6. XPS result of millisecond laser ablation product

Figure 7. TEM result of femtosecond laser ablation product

Figure 7 (a). Deformation structure and its diffraction pattern

Figure 7 (b). Nanocrystalline structure and its diffraction pattern

Figure 7 (c). Nanocrystalline and amorphous structures and their diffraction patterns

Figure 8. TEM result of picosecond laser ablation product

Figure 8 (a). Deformation structure and its diffraction pattern

Figure 8 (b). Deformation and nanocrystalline structures and their diffraction pattern

Figure 8 (c). Nanocrystalline and amorphous structures and their diffraction pattern

Figure 9. TEM result of millisecond laser ablation product

Figure 9 (a). Twin crystal and its diffraction pattern

Figure 9 (b). Nanocrystalline structure and its diffraction pattern

Figure 9 (c). Nanocrystalline and amorphous structures and their diffraction patterns

Figure 9 (d). Amorphous particles and its diffraction pattern

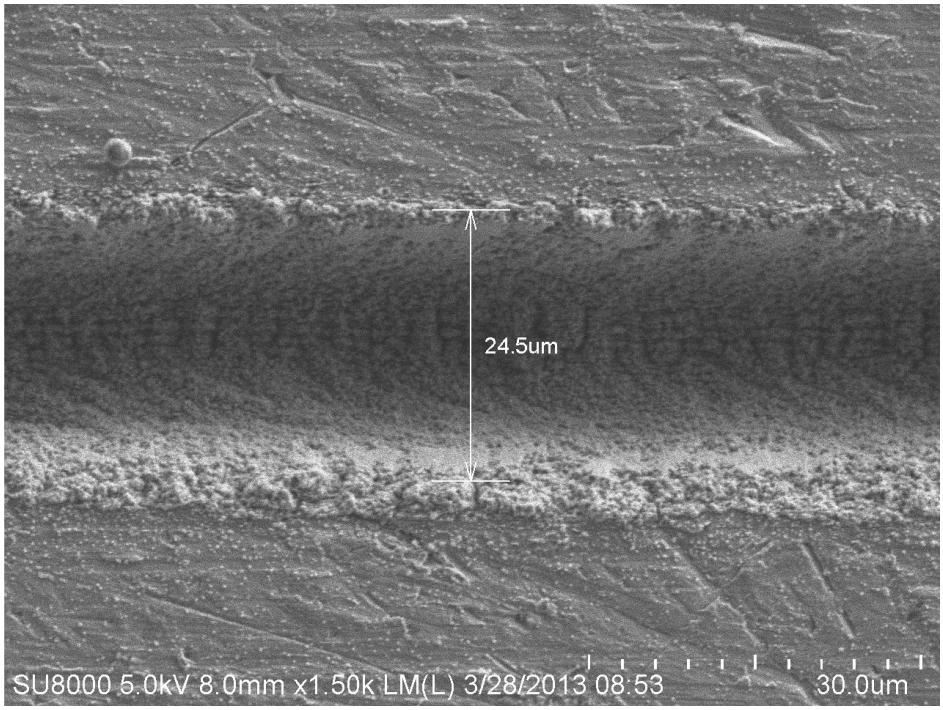

Figure 1 (a). 2-dimensional surface morphology

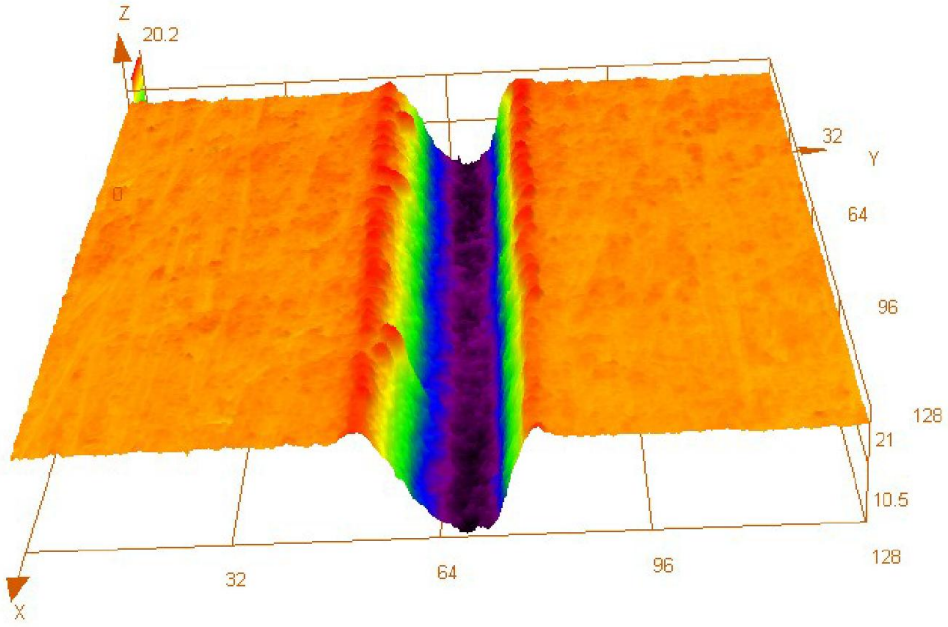

Figure 1 (b). 3-dimensional topography

Figure 1. LSCM results of femtosecond laser ablation product

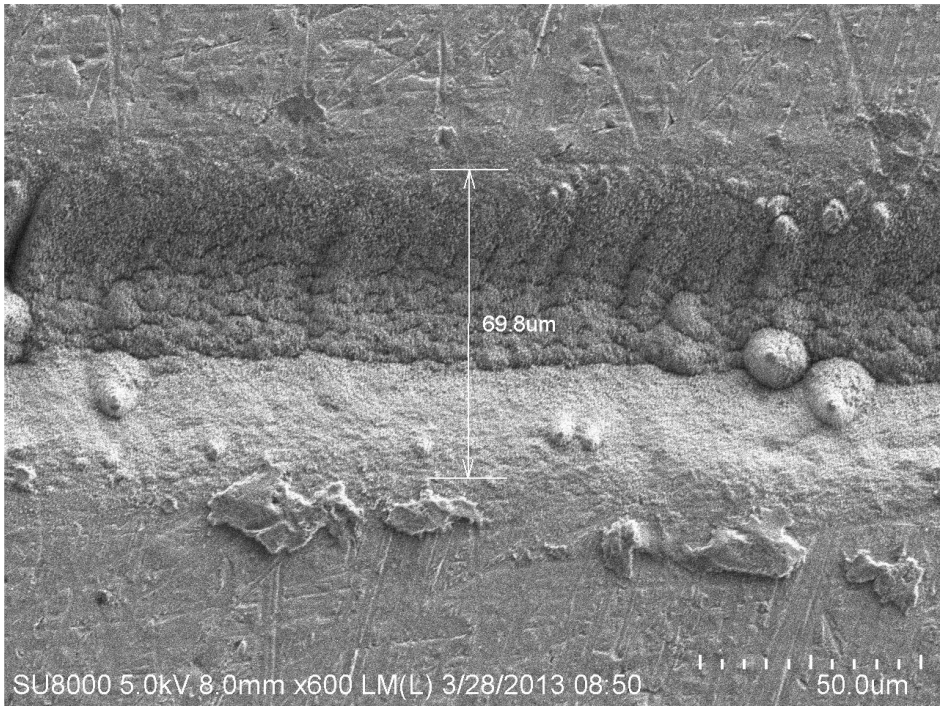

Figure 2 (a). 2-dimensional surface morphology

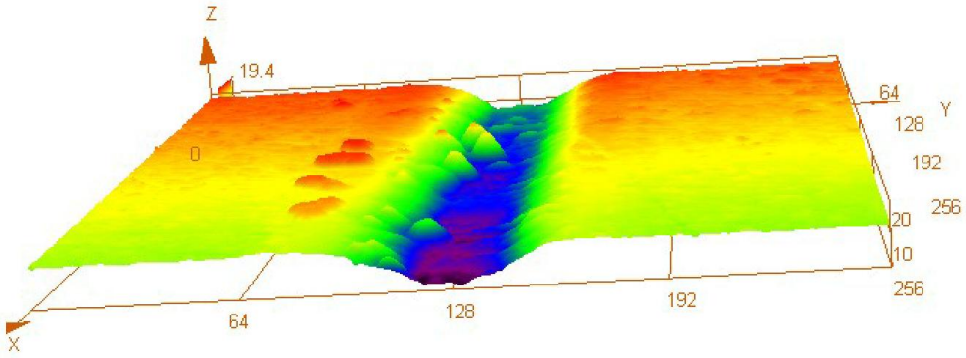

Figure 2 (b). 3-dimensional topography

Figure 2. LSCM results of picosesecond laser ablation product

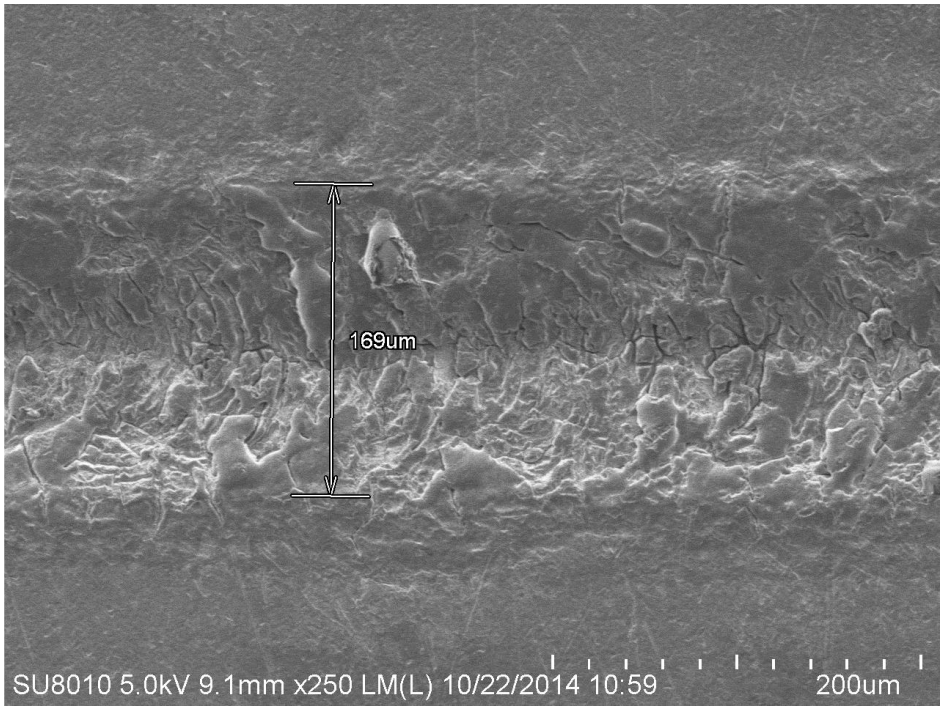

Figure 3 (a). 2-dimensional surface morphology

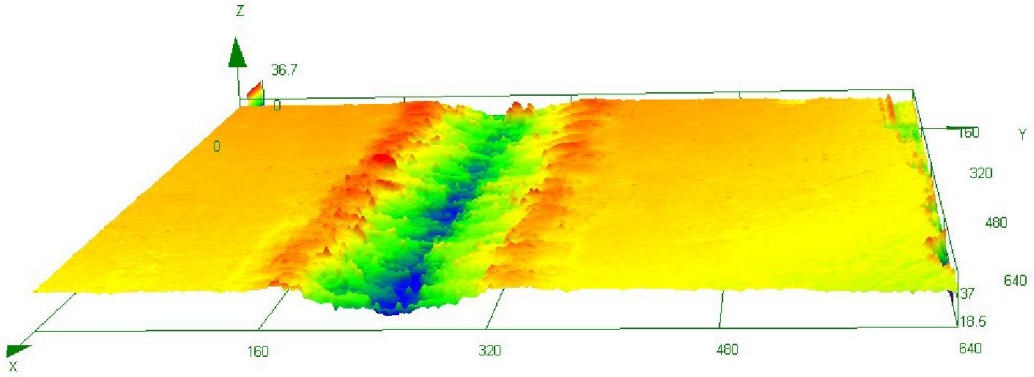

Figure 3 (b). 3-dimensional topography

Figure 3. LSCM results of millisecond laser ablation product

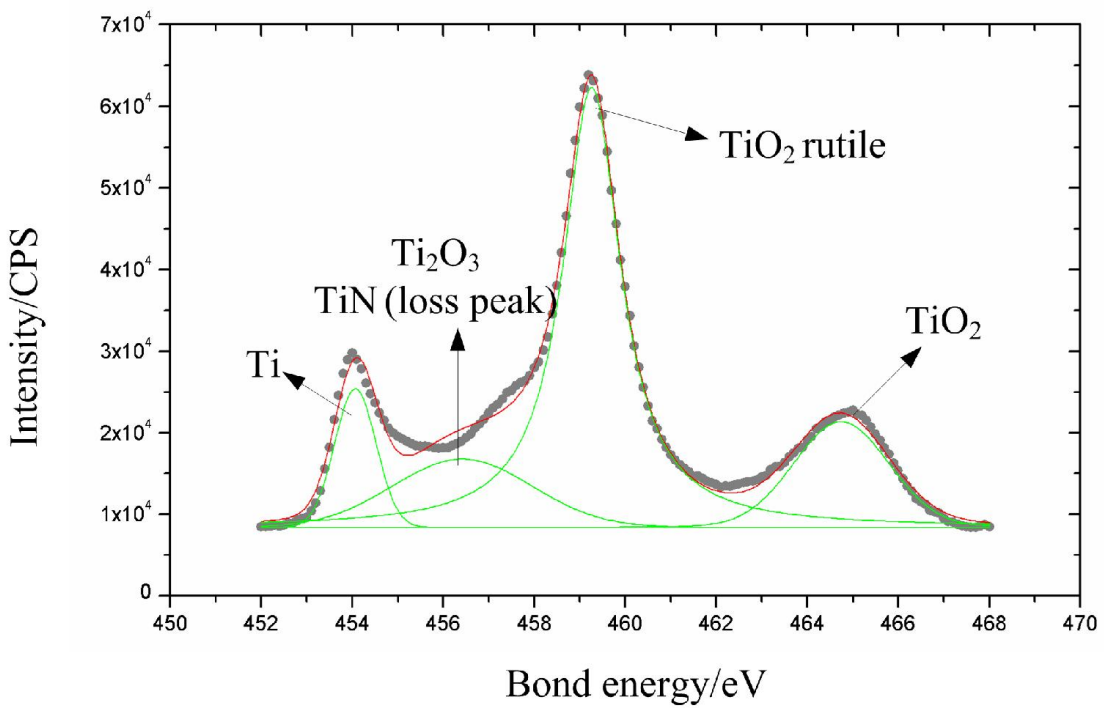

Figure 4. XPS result of femtosecond laser ablation product

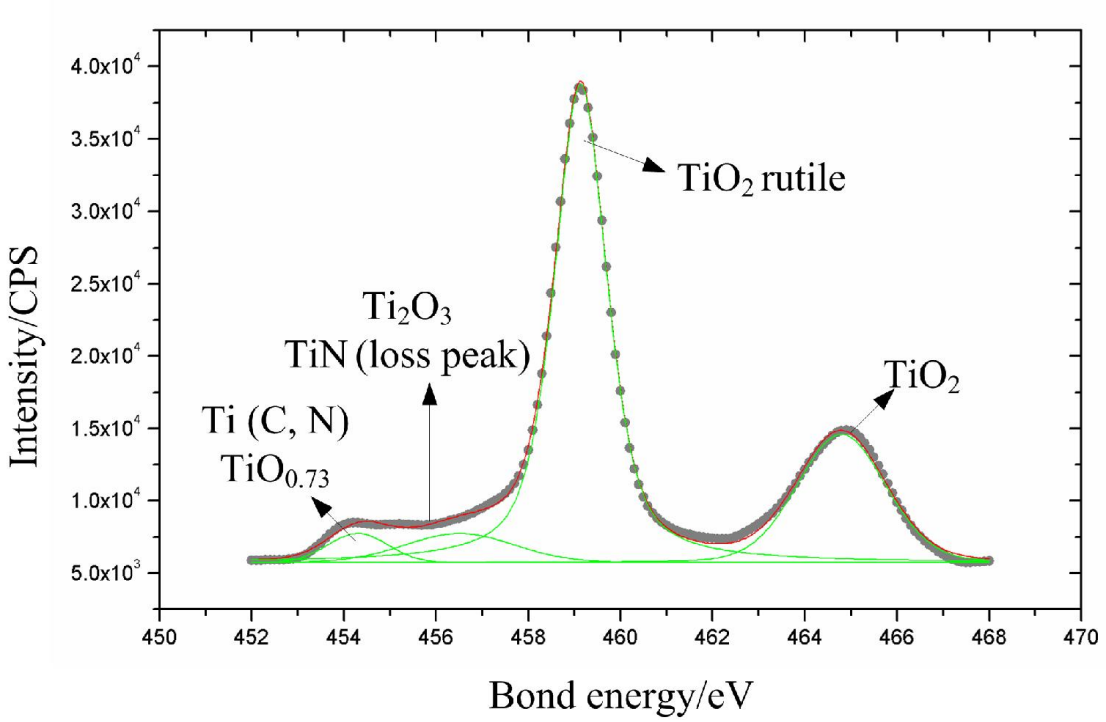

Figure 5. XPS result of picosecond laser ablation product

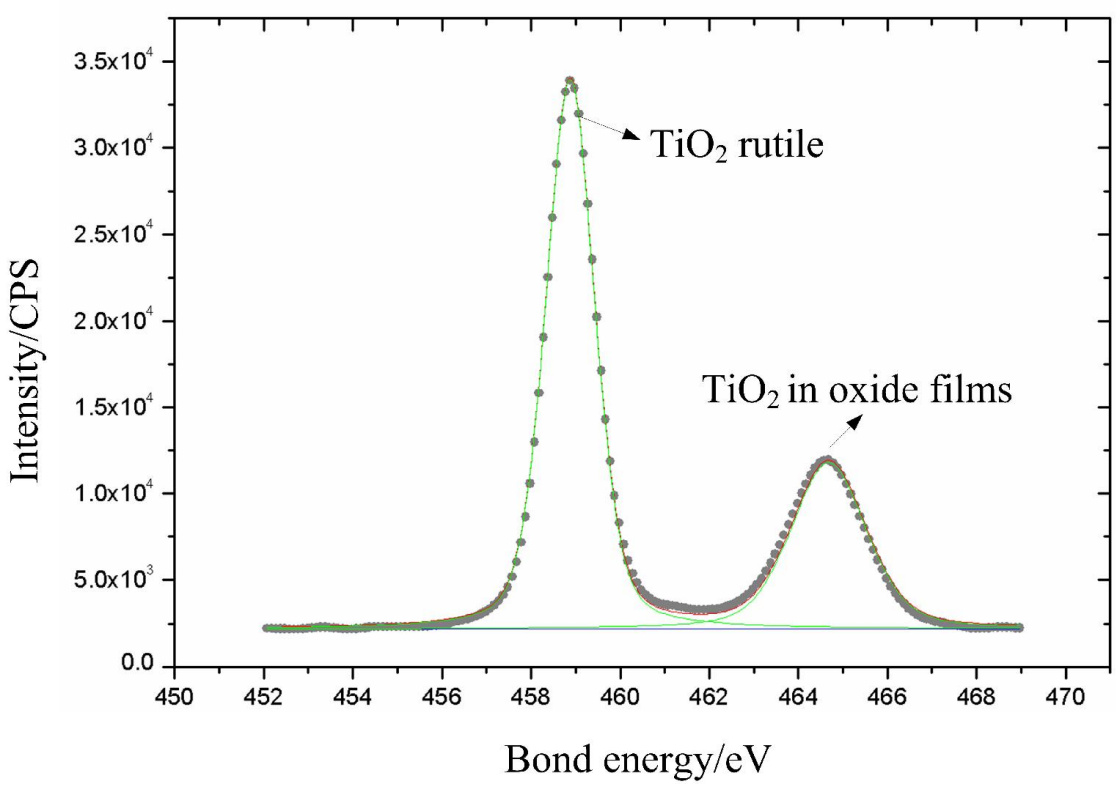

Figure 6. XPS result of millisecond laser ablation product

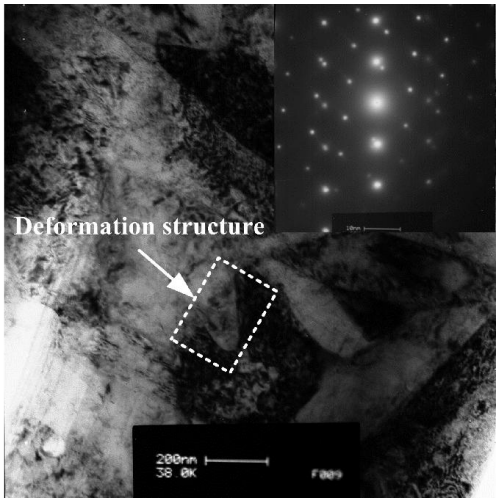

Figure 7 (a). Deformation structure and its diffraction pattern

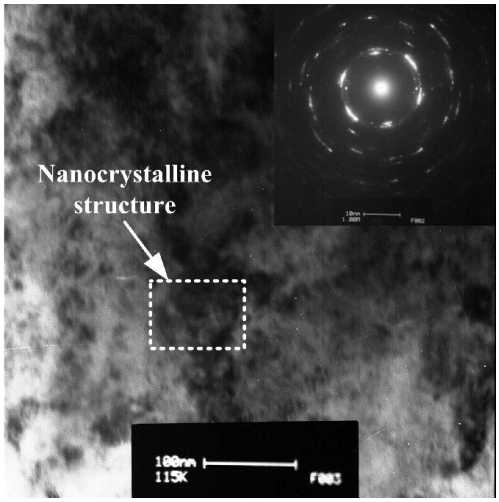

Figure 7 (b). Nanocrystalline structure and its diffraction pattern

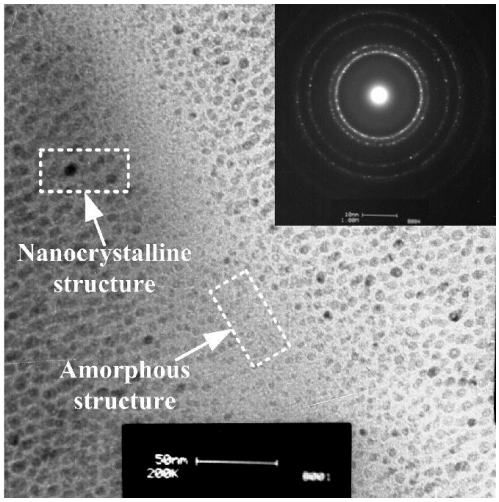

Figure 7 (c). Nanocrystalline and amorphous structures and their diffraction patterns

Figure 7. TEM result of femtosecond laser ablation product

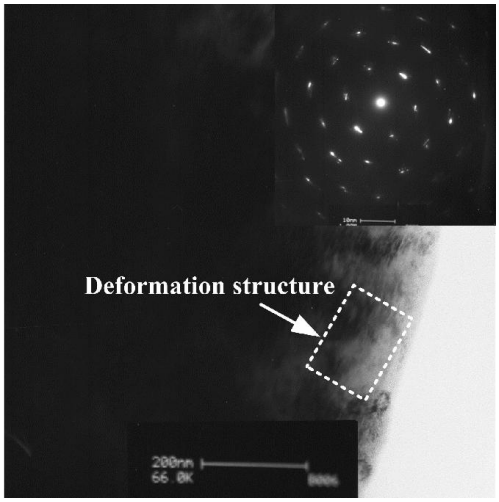

Figure 8 (a). Deformation structure and its diffraction pattern

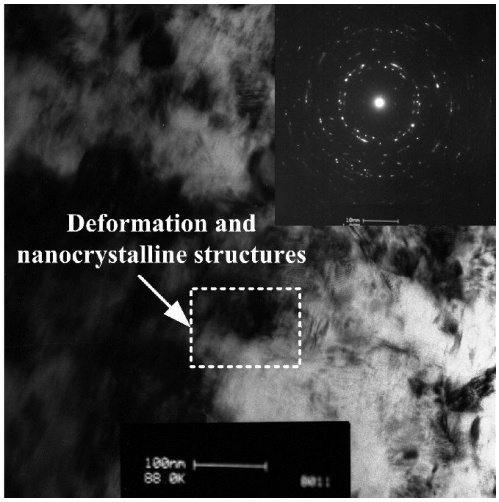

Figure 8 (b). Deformation and nanocrystalline structures and their diffraction pattern

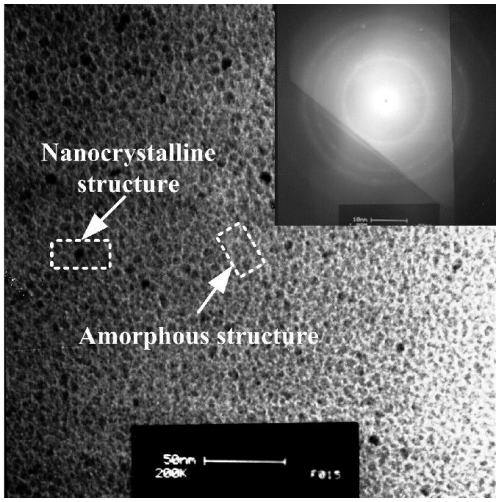

Figure 8 (c). Nanocrystalline and amorphous structures and their diffraction pattern

Figure 8. TEM result of picosecond laser ablation product

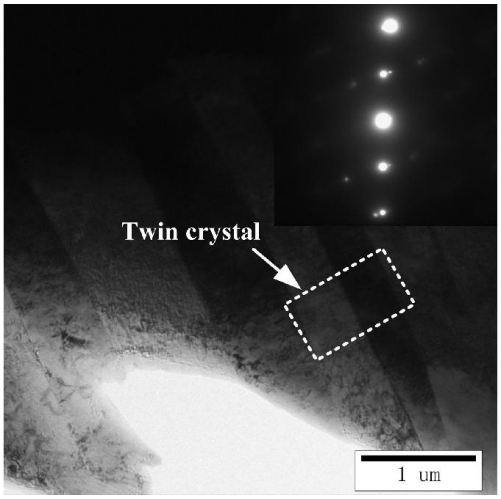

Figure 9 (a). Twin crystal and its diffraction pattern

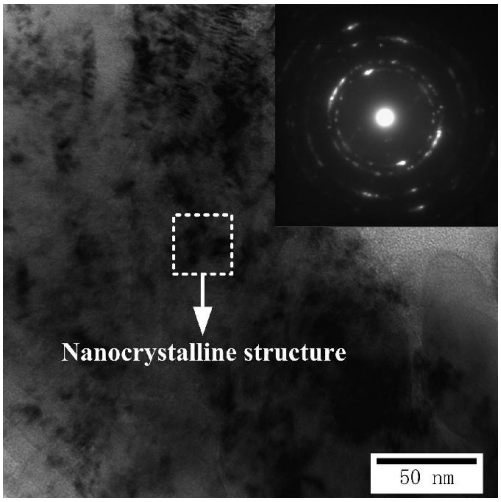

Figure 9 (b). Nanocrystalline structure and its diffraction pattern

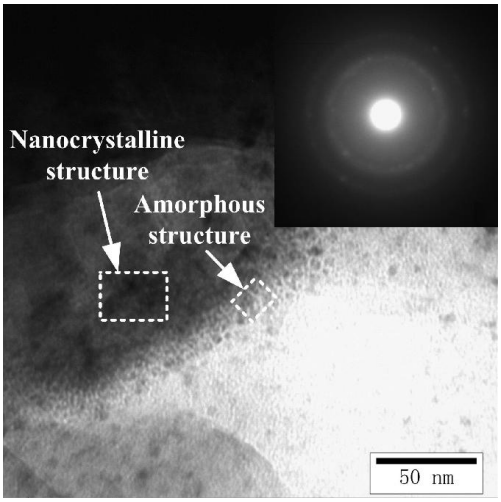

Figure 9 (c). Nanocrystalline and amorphous structures and their diffraction patterns

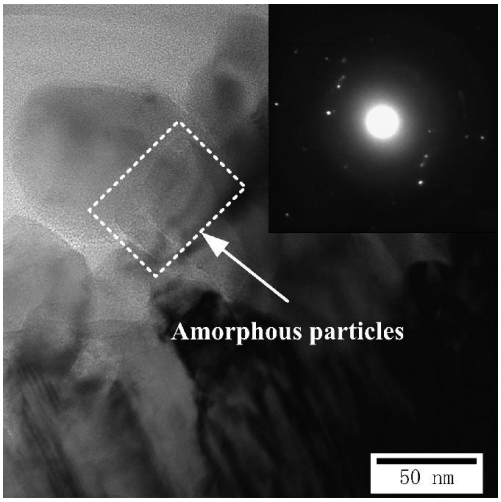

Figure 9 (d). Amorphous particles and its diffraction pattern

Figure 9. TEM result of millisecond laser ablation product